Available online at www.sciencedirect.com
ScienceDirect
Acta Materialia 57 (2009) 5848–5861
Acta MATERIALIA
www.elsevier.com/locate/actamat

An enhanced continuum model for size-dependent strengthening and failure of particle-reinforced composites

Yeong Sung Suh [a,1], Shailendra P. Joshi [b,*], K.T. Ramesh [c]

[a] Department of Mechanical Engineering, Hannam University, Daejeon 306-791, Republic of Korea
[b] Department of Mechanical Engineering, National University of Singapore, Singapore
[c] Department of Mechanical Engineering, The Johns Hopkins University, Baltimore, MD 21218, USA

Received 28 July 2009; accepted 4 August 2009
Available online 10 September 2009

Abstract

We present an enhanced continuum model for the size-dependent strengthening and failure of particle-reinforced composites. The model accounts explicitly for the enhanced strength in a discretely defined "punched zone" around the particle in a metal matrix composite as a result of geometrically necessary dislocations developed through a mismatch in the coefficients of thermal expansion. We incorporate the punched zone explicitly through a unit-cell model within this work, but the approach can be used more generally to account for discrete particle distributions and particle shapes. Smaller particles lead to greater strengthening, and this size effect is larger for larger volume fractions. An equation for the coupling of the size-dependent increase of yield strength of metal matrix composites with the particle volume fraction is obtained. The results indicate that the punched zone effect may amplify the occurrence of a variety of failure modes such as matrix localization, particle fracture and/or particle–matrix interface failure; smaller particles perceive higher stresses. We account for interface failure through a cohesive approach, and show that the interface damage mechanism is also particle-size-dependent. Some implications are presented for microstructural design of metal matrix composites.

Keywords: Particle-reinforced composites; Geometrically necessary dislocations; Punched zone; Enhanced continuum model; Interface failure

1. Introduction

Elastically stiff, non-deformable particle reinforcements with average size in the range of several microns have long been used to enhance the elastic stiffness and yield strength of lightweight structural metals. Conventional metal matrix composites (MMCs) usually have relatively large particles (~30–50 μm) and use high particle volume fractions ($f > 30\%$) to achieve higher strengths, but this is detrimental to the overall ductility. Experimental observations indicate that (for a fixed particle f) the yield strength of such MMCs increases with decreasing particle size (e.g. [1–3]). This raises a promising prospect of using smaller particles and low volume fractions compared to conventional MMCs to achieve high strengths and retain ductility. Arsenault and Shi [1] proposed a model based on prismatic punching of dislocations around the particle, suggesting that this particle-size-dependence is due to a geometrically necessary dislocation (GND) density to accommodate the plastic strain arising from the mismatch in the coefficient of thermal expansion (CTE) [4]. Plastic strain gradients that arise during deformation also produce GNDs [5] due to the elastic–plastic mismatch at the particle–matrix interfaces, although this contribution to the yield strength seems to be significantly smaller than that due to the CTE mismatch [6]. These GND arguments introduce a microstructural length-scale in the otherwise length-scale-independent

* Corresponding author. Address: Department of Mechanical Engineering, National University of Singapore, 9 Engineering Drive 1, Block EA-07-26, Singapore 128040, Singapore. Tel.: +65 6516 4496; fax: +65 6779 1459.
E-mail address: shailendra@nus.edu.sg (S.P. Joshi).
[1] Work performed during sabbatical at the Department of Mechanical Engineering, The Johns Hopkins University, Baltimore, MD 21218, USA.

1359-6454/$36.00
doi:10.1016/j.actamat.2009.08.010

plasticity framework that predicts particle-size-dependent strengthening.

The strengthening from the GNDs due to thermal quenching is sometimes assumed to be distributed over the entire matrix volume so that these dislocations are then counted as part of the background (statistically stored) dislocation density [5,7]. However, this may be a reasonable assumption only in special cases, e.g. a high volume fraction (>20%) of uniformly distributed spherical inclusions (see Appendix A). The dislocation punching distances that delineate the spatial extent of the enhanced hardening are smaller than the interparticle spacing for a range of particle sizes and volume fractions of interest in some of the novel MMCs. This may be especially true for advanced MMCs that exhibit super-high strengths even at relatively low particle volume fractions (e.g. [8]). Also, the GNDs are likely to be distributed non-uniformly owing to non-spherical inclusion shapes. Experimental evidence (e.g. [9]) exists for concentrated dislocations near the ends of cylindrical whiskers that punch out to a distance of several whisker diameters.

There are three characteristics of the GND density that are important in understanding the behavior of MMCs. First, the GNDs will in general not be distributed uniformly through the matrix, but rather will tend to aggregate close to the reinforcing particles, and the distance that they propagate (on average) away from the particles establishes a length-scale inside the material. Second, depending on the shape of the reinforcing particle and the anisotropy of the matrix, the GNDs will often be distributed in a non-symmetric or anisotropic fashion around the particle (e.g. concentrating near the ends of whiskers). Third, non-uniform spatial distributions (i.e. clustering) of the reinforcing particles can result in anomalous GND densities (i.e. non-uniform spatial distributions of GNDs can arise due to the inclusions themselves being clustered in regions of the matrix). While this may adversely affect the overall composite strength, a more striking implication is on the nucleation and growth of different microstructural failure modes [10,11]. In this paper, we consider only the first of these three characteristics (the length-scale associated with the GND distributions). We avoid the second characteristic by considering only spherical particles, and we neglect the third characteristic by assuming a periodic array of the reinforcing particles in the matrix.

We are also interested here in the failure of MMCs, which are known to show a number of distinct failure modes, e.g. particle–matrix interface failure (debonding), matrix failure (void growth and/or strain localization) and particle fracture. Inclusions that strengthen the matrix are also highly likely sites for nucleation of this variety of microstructural failure modes [1]. Clustering of GNDs will also influence the immediate neighborhood and mediate failure processes. For example, Dai et al. [12] showed experimentally and analytically that the additional strengthening due to GNDs may accentuate adiabatic shear localization at high loading rates. Rate-dependent failure response varying from catastrophic shear cracking at quasi-static strain rates ($\sim 10^{-3}\ s^{-1}$) to gradual softening due to microcracking and shear softening at high strain rates ($>10^{3}\ s^{-1}$) is also observed in nano–micro ("trimodal") particulate composites [8].

Failure initiation is inherently a localized phenomenon and homogenized approaches (e.g. Mori–Tanaka mean-field theory) may not be amenable to modeling such effects as they do not account for the effect of actual particle distributions. In addition, most unit-cell and real microstructural models that investigate the influence of the residual stress due to thermal quenching (e.g. [13]) do not account for the particle-size effect, and some other models (e.g. [7]) that do account for the particle size ignore the discreteness of the punched zones where GNDs concentrate due to thermal quenching. In these first results, we ignore the effect of residual stresses, although we recognize that they may be important in determining the tension–compression asymmetry in composites.

In this paper, we investigate the size-dependent micromechanics of failure in MMCs by enriching the classical continuum approach with dislocation-based micromechanics but in a formulation that is easily implemented in elasto-plastic finite-element calculations. The fundamental idea followed in this approach is that the GNDs that emanate as a result of thermal quenching and the CTE mismatch between the constituents are responsible for a heavily dislocated volume (the punched zone) that surrounds individual particles. The resulting additional dislocation density in this region is calculated using the size of the punched volume (e.g. [14]). Thus, apart from the particle size, the size of the punched zone is the additional microstructural length-scale, which does not exist in conventional unit-cell models. It is calculated as a function of the particle size and matrix properties [15]. The punched zone size and its additional dislocation density appear in the computational model as the matrix phase around the particle that has higher strength than rest of the matrix. A non-local interaction arises naturally as the particles and their surrounding punched zones interact with their neighbors through the evolving stress-fields. An early analytical approach to such a model was presented by Maire et al. [16], and we note that composite models that explicitly incorporate an interphase are well known (e.g. [17,18]). Our computational approach retains the capability to model regular and irregular particle distributions while accounting for particle-size-dependence using appropriate physics. We demonstrate that in the absence of damage this model predicts particle-size-dependent strengthening that compares well with experiments, especially at small strains. Further, we investigate the influence of GNDs on a particular mode of failure—the debonding of the particle–matrix interface.

The next section briefly describes the theoretical approach that we adopt to calculate the GND density and the punched zone size. We focus in this paper on a regular particle arrangement instead of a "real" spatial distribution and approximate a cubic arrangement of spherical

particles through an axisymmetric augmented unit-cell finite-element model. The punched zone in the augmented model is represented as a fixed fraction of the matrix endowed with higher strength (due to the GNDs) than the rest of the matrix. Our objective is to probe salient features of the size-dependent failure and extract general inferences rather than specific variations due to specific microstructures. We begin by assuming a perfect interface between the matrix and the particle that captures the overall size-dependent strengthening in the composite. Next, we incorporate an imperfect interface (through cohesive surfaces that may debond) to capture the size-dependent interface debonding. Observations from the numerical simulations for both the perfect and imperfect interface conditions provide useful insights, and we discuss the implications of these results for the design of materials.

2. Dislocation punching micromechanics

Large stresses are induced in an MMC during thermal quenching due to the thermoelastic mismatch between the particle and the matrix. When the stress exceeds the yield strength, dislocations are punched out into the matrix to accommodate the deformation and this also partly relaxes the stress build up; these changes are geometrically necessary in the context of the Ashby's model [19]. Mori and coworkers [15,20] examined the punching of prismatic loops from particles and fibers using Eshelby's inclusion theory. Dunand and Mortensen [14] performed experimental and analytical investigations on the punching distances and strengthening in pure single crystals with spherical and cylindrical reinforcements. Shibata et al. [15] calculated the punching distance of the GNDs using a combined plastic energy dissipation and Eshelby theory, accounting for the effect of the particle volume fraction. We employ the approach in Ref. [15] to calculate punching distances and choose the particle diameter range to be from 1 to 32 μm, idealizing surrounding material as an isotropic continuum.

We note here that there are two possible sources of GNDs. The first is the primary one discussed here, and represents the dislocations that are punched out into the matrix (as a result of the CTE mismatch between particle and matrix) when the composite is cooled down from the processing temperature. From an analytical viewpoint these are usually treated as though they have redistributed themselves over the entire matrix to form a background dislocation density [5,7]. However, the work of Shibata et al. [15] shows that this is not generally the case, and that these GNDs will redistribute over a length-scale l_z; redistribution is only a reasonable approximation when l_z is equal to or larger than the spacing between the particles (Fig. 1a). This discreteness of the GND redistribution should be accounted for in micromechanics of composites. The second source of GNDs is the plastic mismatch, i.e. it is a result of the deformation-induced plastic strain gradients that arise when the composite is plastically deformed (because the matrix deforms plastically but the particles

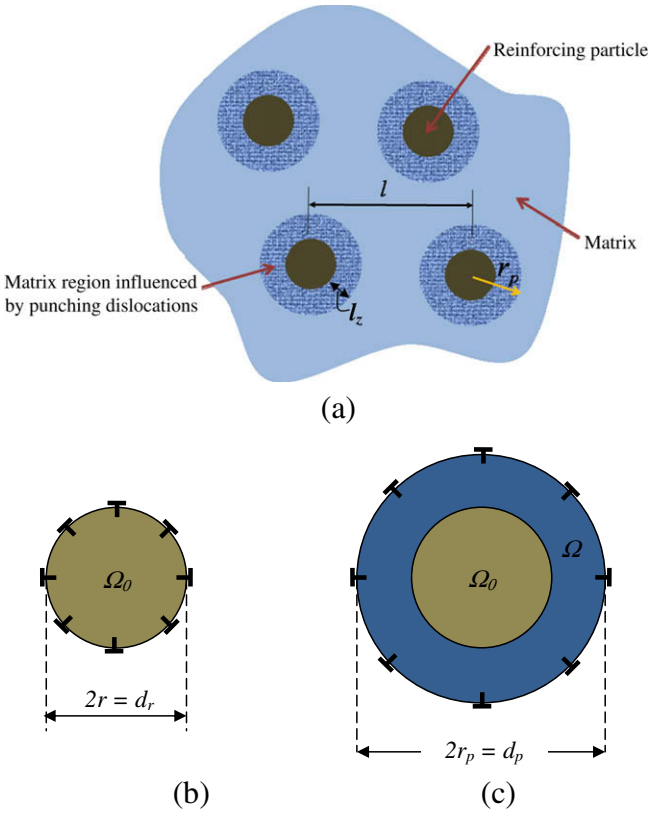

Fig. 1. (a) Schematic illustrating discrete distribution of punched regions around individual particles setting up a microstructural length-scale. (b) Thermal quenching causing prismatic punching dislocations loops at the occurrence of yield near the particle matrix boundary due to CTE mismatch. (c) Location of the punched zone boundary corresponding to equilibrium location of punched dislocations [15]. Ω_0, spherical particle domain; $\Omega - \Omega_0$, punched domain.

do not). Many of the strain gradient plasticity models in the literature for size-dependent strengthening in particle-reinforced composites only explicitly consider this second source of GNDs. While this source of strengthening contributes at large strains, it is not likely to be significant at small plastic strains immediately following yield [6] and this is also illustrated in Appendix B for one of the simulated unit-cell calculations. At such strains, we confirm that the dominant contribution to particle-size-dependent strengthening comes from the thermal quenching stress.

2.1. Density of excess dislocations

We assume that the excess density due to the GNDs is uniformly distributed in a spherical shell called the punched zone of volume (V_z) size l_z, bounded by an outer radius r_p (calculated in the next section) and inner radius, r, the particle radius. Based on Ashby's model the total dislocation line length (L) due to N number of dislocations punched out from a spherical particle–matrix interface is [19]:

$$L = 2\pi r N = \frac{8\pi r^2 \varepsilon_p}{b} \approx \frac{k\pi r^2 (\Delta\alpha \Delta T)}{b}, \tag{1}$$

where b is the magnitude of the Burgers vector, $\Delta\alpha = \alpha^* - \alpha$ is the CTE mismatch with α^* being the CTE of the particle and α that of the metal matrix, and ΔT is the temperature change. The parameter k accounts for the geometry and plastic part of the total thermal strain responsible for the dislocation punching. This gives the excess dislocation density ρ_g in the punched zone:

$$\rho_g = \frac{L}{V_z} = \frac{A' r^2 (\Delta\alpha \Delta T)}{b(r_p^3 - r^3)} \tag{2}$$

where the parameter A' is of order 10 [2] [14,19]. To use this relation one must have r_p, the size of the punched zone, and this is discussed next.

2.2. The size of the punched zone

We employ the equations of Shibata et al. [15] based on the Eshelby inclusion theory to calculate the punched zone size. An attractive feature of their formulation is that it accounts for the effect of other particles (essentially the volume fraction) on the punching distance. The origin of these prismatic dislocations (Fig. 1b) is the CTE mismatch between the particle and the matrix and the temperature change, ΔT, between the processing and room temperatures. Assuming spherical symmetry, the punching distance (r_p) from the center of the particle is:

$$r_p = r\left\{\frac{B(1-2Pf) + \sqrt{B^2(1-2Pf)^2 + 16\left(\frac{\tau_y}{G}\right)PB}}{\left(\frac{4\tau_y}{G}\right)}\right\}^{\frac{1}{3}} \tag{3}$$

where r is the particle radius and f is the volume fraction of the particles. The coefficients B and P are determined from the elastic coefficients and the thermal mismatch as:

$$B = \frac{(1+\nu)|\Delta\alpha\Delta T|}{(1-\nu)} \tag{4}$$

and

$$P = \frac{2(1-2\nu)(3\bar{\lambda} + 2\bar{G})}{(1-\nu)[(1-f)(3\bar{\lambda} + 2\bar{G})\left(\frac{1+\nu}{1-\nu}\right) + 3\{f(3\lambda^* + 2G^*) + (1-f)(3\lambda + 2G)\}]} \tag{5}$$

Here the asterisked material quantities are those for the particle and the plain ones are those for the matrix. In Eqs. (2)–(4), τ is the shear yield strength, ν is the matrix Poisson's ratio, and $\bar{\lambda} = \lambda^* - \lambda$, $\bar{G} = G^* - G$ are the mismatches of the Lame constants. The punched dislocations create a region around each particle whose extent is affected by its surrounding particles through the volume fraction f. For a given material, smaller volume fractions f (i.e. larger interparticle distances) and larger particle diameters ($d_r = 2r$) could result in punching distances (r_p) large enough to occupy the entire matrix region of the unit-cell or even cause the neighboring punched regions to overlap. In this paper, we restrict our attention only to those combinations of f and r in which such situations do not arise. For most of the particle sizes under consideration here, this restricts the model to volume fractions that are less than 20% ($f < 20\%$).

2.3. Strengthening in the punched zone

Using Eq. (2), the strength of the material within the punched zone due to the GND density is:

$$\sigma = \sigma_y + aGb\sqrt{\rho_g}, \tag{6}$$

where $a = 1.25$ for aluminum [21]. The dislocation density (Eq. (2)) in the plastic zone is presented in Fig. 2 as a function of the particle volume fraction and the particle diameter. A dramatic increase in the dislocation density is observed for particles less than 5 μm diameter, whereas the volume fraction effect, though present, is not as significant. Fig. 2 demonstrates that there is a strong strengthening effect within the punched zone as the particle size decreases, and as a consequence one should expect a strengthening of the overall composite. We determine the overall behavior of the composite incorporating this "enriched continuum" response through a computational approach, which is described in the next section. We consider two distinct scenarios. In the first, the composite is assumed to sustain no damage, while in the second we account for particle-size effects on interface failure.

3. Computational approach

We consider a regular array of spherical elastic particles in an elastic–plastic metal matrix using an axisymmetric unit-cell modeled with finite elements (using Abaqus [22]). The axisymmetric unit-cell model is a practical and effective approximation that has been extensively used to analyze the mechanical behavior of particulate composites [23,24]. The unit-cell (Fig. 3a) contains the particle, the punched zone and the matrix. The particle size and volume fraction are independently controlled, and the punched

[2] For simplicity, we use $A' = 6\sqrt{2}$ in line with Ref. [14], but note that the value of A' may change to accommodate the nature of the particular matrix of interest (e.g. the homogenization associated with a polycrystalline matrix).

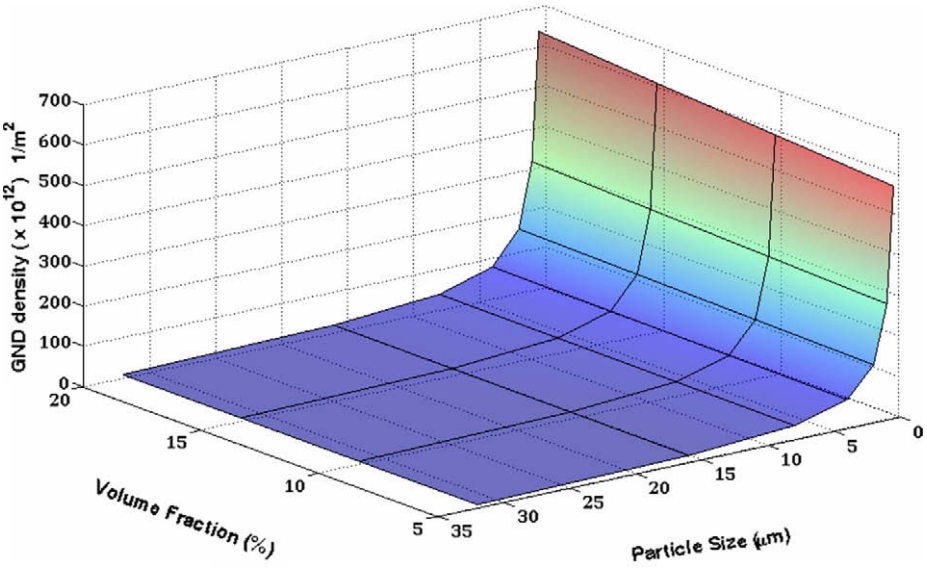

Fig. 2. Excess dislocation density in the punched zone as a function of the volume fraction and the spherical particle diameter for the case of the SiC/A356 composite.

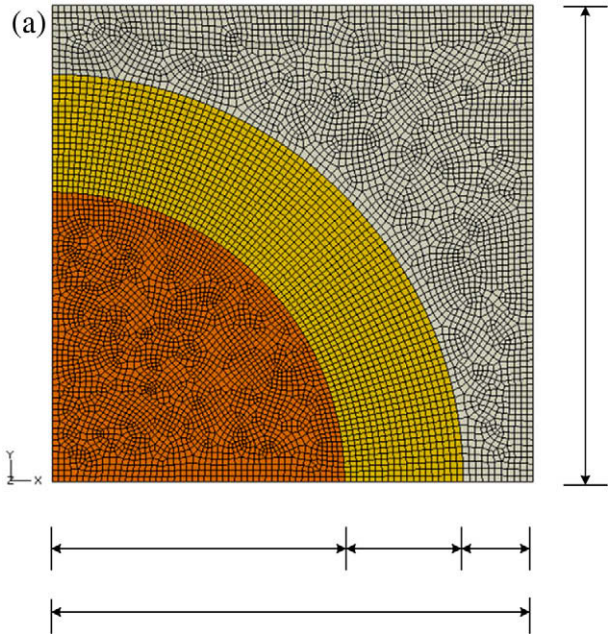

Fig. 3a. Finite-element mesh of an axisymmetric unit-cell for the case of the perfectly bonded particle–matrix interface. The unit-cell is similar for the imperfect interface, except that the mesh is finer

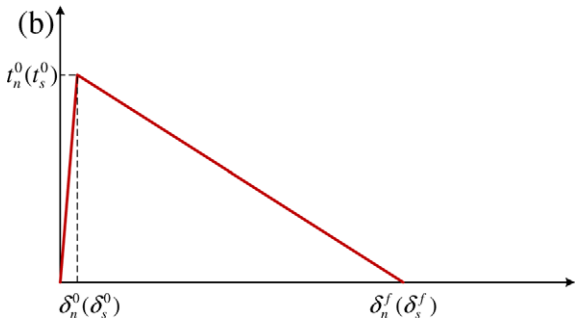

Fig. 3b. Assumed traction-separation behavior of the interface for the case of interface debonding, showing both tension and shear on the same axes.

zone size is prescribed using Eq. (2). The interface between the matrix and the particle is modeled both with and without interfacial debonding (the former uses the cohesive zone approach, Fig. 3b, discussed later in the paper). Symmetry boundary conditions are imposed along the x and y axes. A uniform displacement in the positive y direction is prescribed along the top boundary, while the right boundary remains traction-free and straight during deformation. The composite true stress ($\bar{\sigma}$) – true strain ($\bar{\varepsilon}$) behavior of the unit-cell is obtained from the extensional displacement u_y and the tensile force F_y generated on the top boundary by using the following equations:

$$\bar{\sigma} = \frac{1}{\pi r_c^2} \int_0^{r_c} F_y|_{y=h_c} dx \tag{7}$$

and

$$\bar{\sigma} = \ln\left(1 + \frac{u_y}{h_c}\right) \tag{8}$$

where h_c is the initial height of the axisymmetric unit-cell (identically equal to its initial radius) and r_c is the current unit-cell radius. For a typical simulation of a perfectly bonded interface, approximately 7000 elements were used, while for the models with interfacial debonding, approximately 10,000 elements were used with a finer mesh near the interface. Mesh convergence was ensured in both the cases.

3.1. Constitutive behavior

3.1.1. Particle and matrix response

In this work, we consider an Al alloy matrix containing SiC particles. The particle reinforcement is assumed to be

isotropic and elastic with Young's modulus $E^* = 427$ GPa, Poisson's ratio $\nu^* = 0.17$, and a CTE of $\alpha^* = 4.3 \times 10^{-6}\ \mathrm{K}^{-1}$ (these properties correspond to SiC, which is the particle in some of Lloyd's experiments). The matrix is isotropic and elastoplastic with $E = 76$ GPa, $\nu = 0.33$, and $\alpha = 23.63 \times 10^{-6}\ \mathrm{K}^{-1}$, the magnitude of the Burgers vector (b) is taken to be 0.28 nm and the initial yield strength, $\sigma_y = 208$ MPa [5]. The plastic hardening behavior of the matrix is described using J_2 flow theory, using as input the uniaxial stress (in MPa)–plastic strain relation: $\sigma = 464(0.00274 + \varepsilon^p)^{0.136}$ based on experimental data in the literature [3,5]. The punched zone is modeled with a similar elastoplastic behavior except that the yield strength is higher than the rest of the matrix (Eq. (6)) with the strengthening determined by a thermal quenching ΔT of 474 K [3]. We note that the Al alloy in the experiments in Ref. [3] was an A356-T6 alloy that contains fine silicon particles, but like previous investigators [5,7] we ignore such substructure and simply use the stress–strain curve as input for our modeling purposes.

3.1.2. Particle–matrix interface behavior

We begin by investigating the behavior of composites with a perfect particle–matrix interface, and then proceed to address the issue of composite damage through interface debonding (interfacial debonding). We do not consider the case of the presence of a real interphase material, focusing instead on the common case of direct interface failure at the particle–matrix interface. Interfacial debonding is modeled using the cohesive surface model in Abaqus (Standard, version 6.8 [22]) that is defined using a traction-separation law. We assume a rigid interface behavior prior to damage; this is achieved by assigning a default penalty for the interface normal and shear stiffnesses. The traction-separation response that we assume for the interface is shown schematically in Fig. 3b, which shows the behavior in both tension and shear on the same axes. The peak value of the contact stress is t_n^0 when the separation is purely normal (and t_s^0 when the separation is tangential), and these correspond to separation distances of δ_n^0 and δ_s^0, respectively. The failure of the interface is characterized by a linear degradation of the cohesive stiffness, until a complete loss of traction occurs at critical separation distances of δ_n^f and δ_s^f in normal and tangential cases, respectively. We assume a quadratic stress criterion for damage initiation in the multiaxial case:

$$\left(\frac{\langle t_n \rangle}{t_n^0}\right) + \left(\frac{t_s}{t_n^0}\right)^2 = 1, \tag{9}$$

where $\langle\rangle$ are the Macaulay brackets (i.e. interface damage commences when the interface tractions satisfy this condition). Under a combination of normal and shear separations across the interface, the effective separation δ_m is defined as:

$$\delta_m = \sqrt{\langle \delta_n^2 \rangle + \delta_s^2}. \tag{10}$$

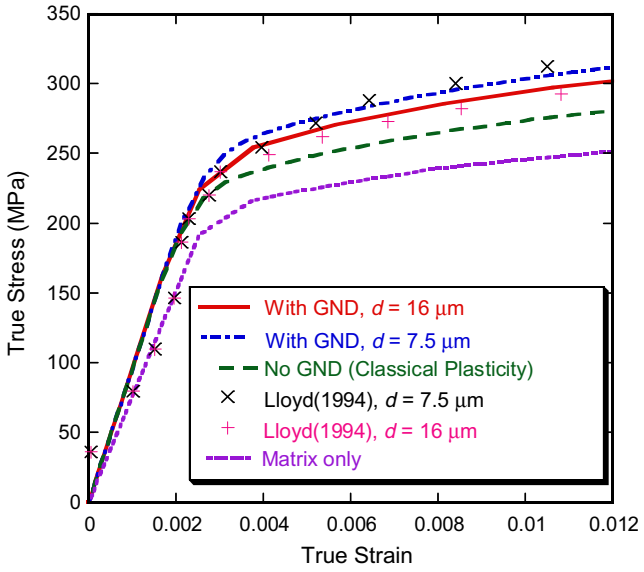

Fig. 4. Comparison of numerical and experimental [15] composite true stress–strain curves for 7.5 and 16 μm SiC particles. For reference, a numerical result corresponding to the classical plasticity is included.

Damage evolution is described through a scalar damage variable D ranging from 0 to 1 that represents the overall damage at a contact point. For the case of linear softening as in Fig. 3b, the scalar damage variable is defined as:

$$D = \frac{\delta_m^f(\delta_m^{\max} - \delta_m^0)}{\delta_m^{\max}(\delta_m^f - \delta_m^0)}, \tag{11}$$

where $\delta_m^{\max}$ refers to the maximum value of the effective separation attained during the loading history and δ_m^f can be obtained using the final separations in Eq. (10). The interface traction components t_n and t_s are affected by the damage as shown in Fig. 3b, essentially following the relations:

$$t_i = \begin{cases} (1-D)\bar{t}_i & \text{if } \bar{t}_i \geqslant 0 \\ \bar{t}_i & \text{otherwise,} \end{cases} \tag{12}$$

where $\bar{t}_i$ ($i = n$ or s) are the contact stress components predicted by the elastic traction–separation behavior for the current separations without damage.

4. Numerical results and discussion

We first discuss the case without damage, with the objective of understanding the size-dependent strengthening of particle-reinforced MMCs. For comparison, we also present model results that do not account for the punched zone effect, i.e. results that are obtained with a unit-cell model (like that in Fig. 3a) in which the entire region outside the particle has just the matrix properties. We refer to the latter model as the conventional plasticity model.

4.1. Particle-size-dependent strengthening

The true stress–true strain ($\bar{\sigma} - \bar{\varepsilon}$) curves predicted by the model are presented in Fig. 4 for A356 Al alloy con-

taining 15 vol.% of SiC particles that are either 7.5 or 16 μm in diameter. The matrix behavior that is the input to the model is shown as the dotted line in the figure. Consider first the computed results using the conventional plasticity model (the long dashed lines). The predicted composite response using conventional plasticity shows the reinforcement strengthening, with both particle sizes providing exactly the same strengthening (as expected). However, the augmented unit-cell model (with the punched zone) predicts a size effect, with the smaller particles providing the greater strengthening at the same volume fraction. These predictions are in good agreement with the experimental results [3], at least for the overall strains shown here (recognizing that damage will develop at some sufficiently large tensile strains in any experiment). Qu et al.'s [5] strain gradient plasticity model also showed a similar comparison with Lloyd's results at small strains. For comparison, we also incorporate the deformation-induced plastic strain gradient effect. However, as seen in Fig. B1 (Appendix B), the plastic strain gradient has no influence on the yield strength and contributes only to the strain hardening.

Note that the stress–strain curves in Fig. 4 are compared at small strains; at larger strains the numerical curves continue to harden while the experimental results exhibit softening, probably due to damage initiation and evolution. We discuss one possible damage mechanism in detail in a subsequent section. The predicted change of the composite response with varying particle size is shown in Fig. 5 for various fixed volume fractions. As expected, the effect of particle size on the yield strength (at 0.2% strain) is small at low volume fractions but is significant at higher volume fractions. For a given volume fraction, the initial work hardening after yield is higher for smaller particles, which agrees well with the observations of Lloyd [3]. Qualitatively similar results were observed by McDanels [25] with Al 6061-T6/SiC, and Llorca et al. [26] with Al 2024-T6/SiC. From the continuum viewpoint, this size-dependent strain hardening results from the fractional proportion of the GND zone in the augmented unit-cell, which further stiffens the overall plastic response. For a constant volume fraction, smaller particles give stronger punched zones, and therefore higher overall hardening. From a dislocation mechanics perspective this behavior may be attributed to the increased forest hardening due to high dislocation density near the particles.

The normalized yield strength (composite yield strength normalized by the matrix yield strength) is shown in Fig. 6 as a function of the volume fraction and particle size, clearly illustrating the coupling between these two microstructural parameters. This coupled dependence of the composite yield strength on the particle volume fraction and size can be described by fitting a simple analytical equation. Such an equation, though rudimentary, could be quite useful in making quick decisions for microstructural design. Using least-squares fit, Eq. (13) is an empirical expression to the computationally derived results of Fig. 6:

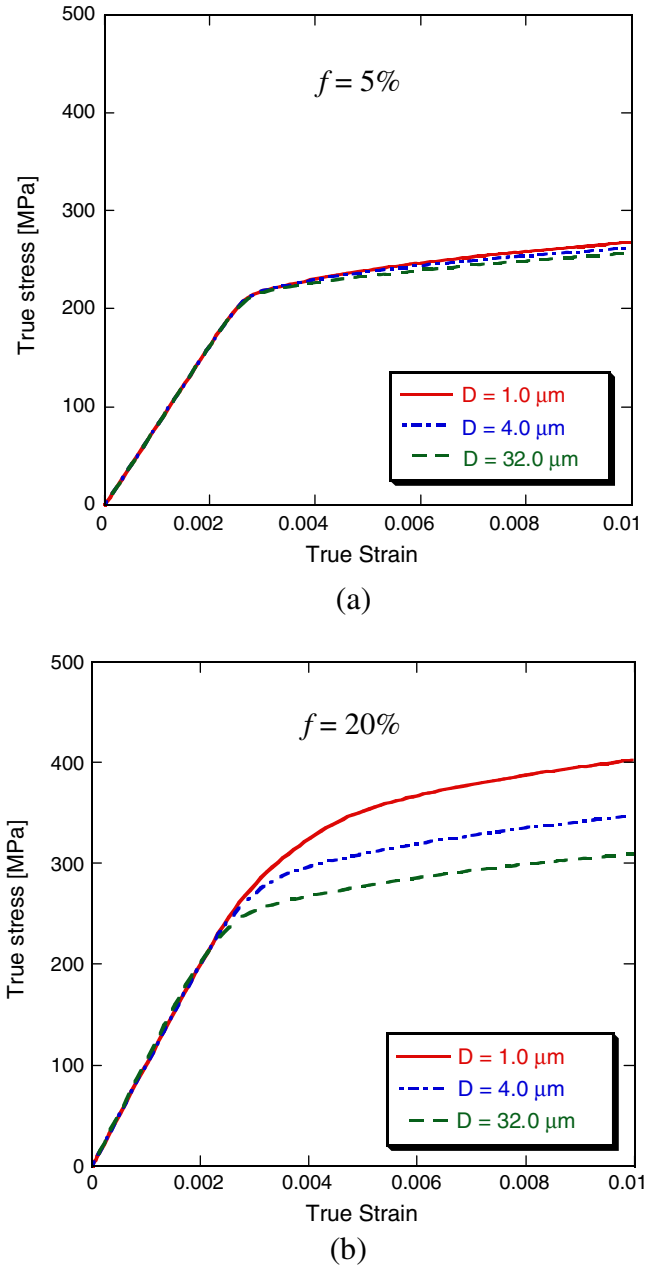

Fig. 5. Composite stress–strain curves for (a) $f = 5\%$ and (b) $f = 20\%$ with different particle sizes (properties correspond to an Al–SiC composite). Note the stronger influence of particle size at high volume fractions, and the increased overall strain hardening of the composite with smaller particles at a given volume fraction.

$$\frac{\sigma}{\sigma_y} = 1 + f^m(A + Bd^n) \tag{13}$$

where m, A, B and n are the fitting parameters (presented in Table 1 for the matrix–particle combination considered here).

The coefficients in Table 1 are valid only for spherical inclusions and will vary for other regularly shaped inclusions, although this might be non-trivial as determining the punched zone shapes and sizes may not be straightforward. We briefly discuss a possible strategy to address this aspect in Appendix A.

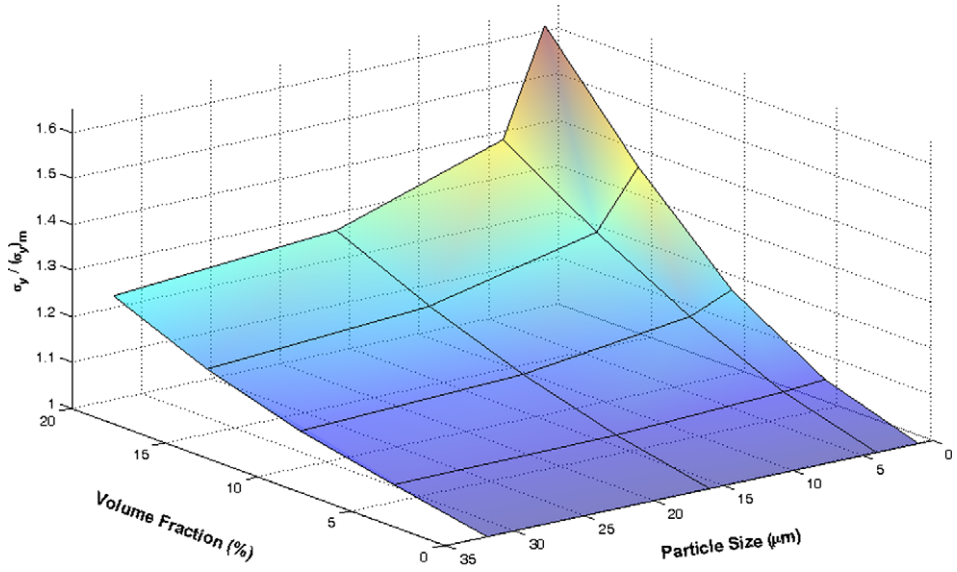

Fig. 6. Normalized composite yield strength (0.2% offset) as a function of particle volume fraction and particle size.

Table 1
Coefficients for Eq. (13).

A	B	m	n
4.03×10^{-4}	2.13×10^{-3}	1.833	−0.38

The computational model predicts very high strengthening (>1.5 times the matrix strength) at moderate f (>12%) especially at small particle sizes ($d_r < 10$ μm). Note that in the absence of the punched zone the surface would be essentially flat along the particle-size axis. The punched zone size is directly proportional to the particle size (Eq. (3)) and gives a higher dislocation density and therefore greater strength in that zone for smaller particles (as the dislocation line length around a particle decreases less rapidly compared to the corresponding decrease in volume). Note that in many materials some form of damage may be initiated at high stresses. In a later section, we plot a similar strength surface in the presence of interface damage.

While the overall behavior of the composite is certainly of interest, much more insight into strengthening and potential failure mechanisms can be obtained from the distributions of the stresses and strains in the composite (unit-cell). Fig. 7a and b compare the von Mises stresses in a 16 μm particle composite with $f = 15\%$, with the strengthened punched zone (Fig. 8a) and without (Fig. 8b, the conventional plasticity model); note the identical mesh is used in the two cases, but the entire matrix has the same properties in Fig. 8b. It is apparent that the particle carries higher stress in the presence of the punched zone than in the conventional plasticity case. This is because under a macroscopic imposed strain of 1%, although both the matrix and the punched zone have undergone plastic deformation in Fig. 7a, the resulting stresses have to be larger in the punched zone compared to the remaining matrix (for this prescribed overall strain). Consequently, the heavily stressed punched zone loads the particle, leading to higher stresses in the particle. This may have significant implications for particle damage.

The influence of particle size on the stress distributions is significant, as shown in Fig. 8. This figure presents the von Mises stress distributions (at 1% strain) in composites made with 1 and 16 μm particles for two volume fractions ($f = 0.05$ and $f = 0.15$). We have performed similar simulations over a wide range of particle sizes and reinforcement volume fractions, and in general, smaller particles with higher volume fractions tend to experience larger stresses. Further, for a given volume fraction the maximum von Mises stress occurs at the particle–matrix interface and is greatly amplified as the particle size decreases. Thus the probability of particle failure and interface failure increases as the particle size decreases. These microscale factors have an important bearing on the size-dependent failure modes in MMCs, which we address in the next two sections. We begin by discussing the possibility of size-dependent interface failure.

4.2. Particle-size-dependent interface failure

As demonstrated in Fig. 4, assuming a perfect interface between the particle and the matrix, the computed overall flow stresses at small strains agree well with experimental results. However, at larger strains, the predicted curves are higher than the experimental ones measured by Lloyd [28], i.e. the flow stress is overestimated. As noted earlier, this discrepancy is likely to arise due to the fact that the computations did not consider the possible activation of failure modes – e.g. particle fracture, particle–matrix interface debonding and/or matrix failure through voiding/strain localization. The occurrence of any of these modes may be further accentuated by the presence of excess

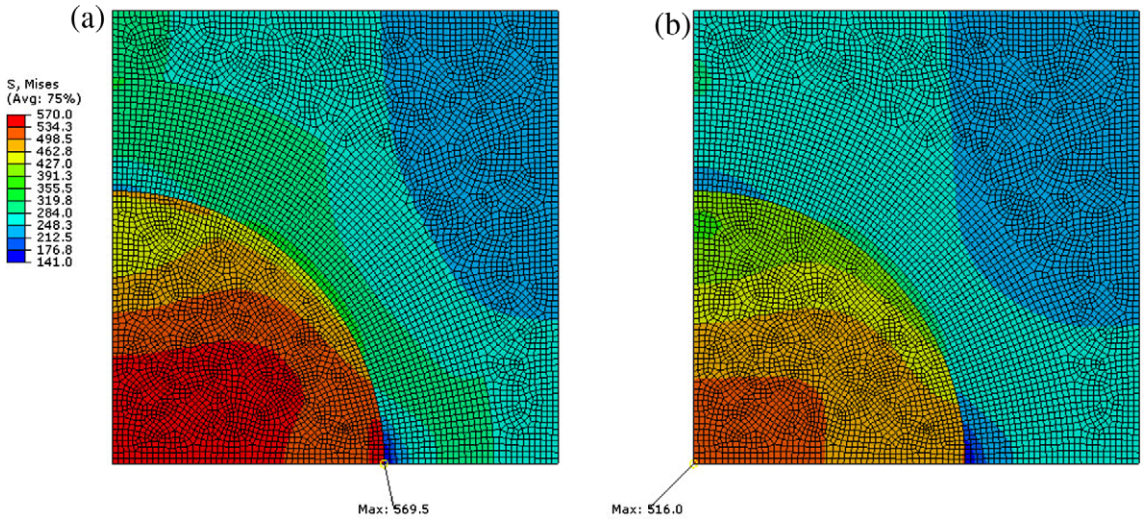

Fig. 7. The von Mises stresses in a 16 μm particle composite with $f = 15\%$: (a) with the strengthened punched zone and (b) without the punched zone (the conventional plasticity model).

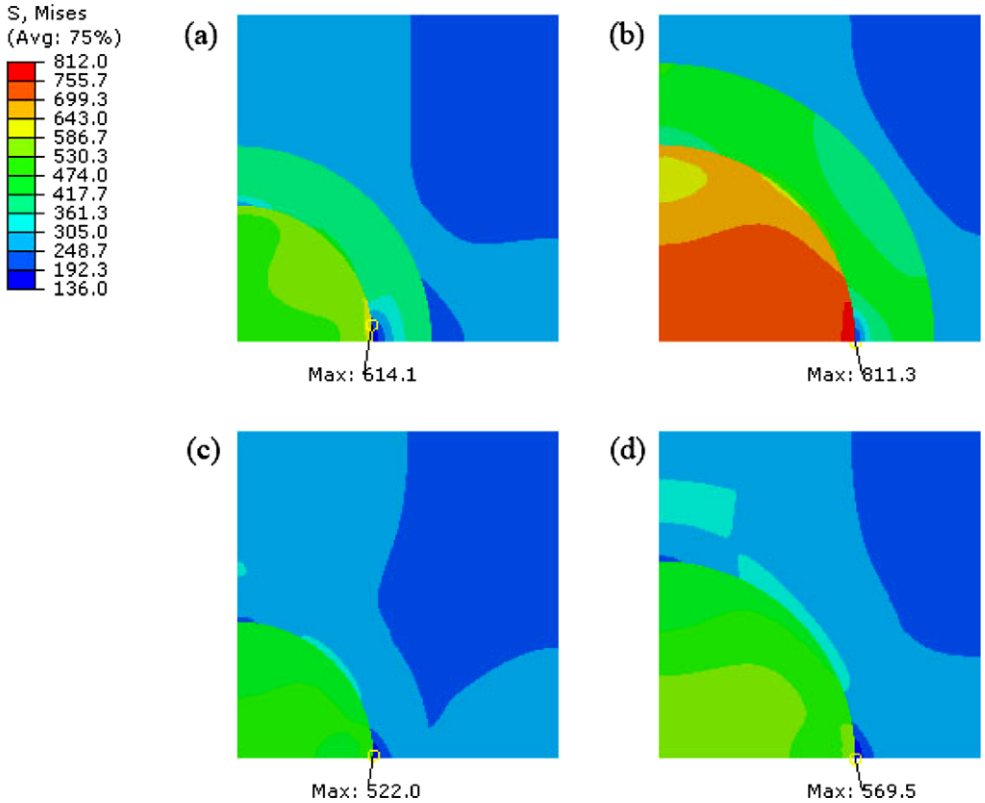

Fig. 8. Distribution of equivalent (von Mises) stress in the augmented unit-cells at 1% strain: (a and b) 1 μm particles, with volume fractions of 5% and 15%, respectively; (c and d) 16 μm particles, with volume fractions of 5% and 15%, respectively. Thus looking vertically, (a) and (c) represent the same volume fraction (5%) but different particle sizes (1 and 16 μm, respectively) and similarly (b) and (d) for the volume fraction of 15%. Note that the highest particle stress and interface stress is in (b), with small particles and large volume fractions.

strengthening. Although multiple modes may be active at a given time, we choose to address in this paper only failure of the interface in the presence of the punched zone, given that this is a common failure mode [3,27–29]. We discuss the implications of the punched zone on other modes of failure in Section 5.

The particle–matrix interface is modeled using cohesive surfaces as described in Section 2. The interface response prior to softening is assumed to be near-rigid by adopting the contact penalty method [19]. The interface parameters for damage initiation and evolution are obtained by fitting our computational results for the overall stress–strain

curve of an A356/SiC composite with 15 vol.% of 16 μm diameter SiC particles to the experimental stress–strain curve provided by Lloyd [3]. The best fit parameters are $t_n^0 = 444$ MPa, $t_s^0 = 222$ MPa, and $\delta_n^f = 1.5$ μm. These parameters are certainly not unique, but we choose them as a representative set to describe the interface behavior and use these parameters for all particle sizes and volume fractions. Mesh convergence is ensured by running the same simulation using finer meshes.

Fig. 9 shows the distribution of the effective plastic strain for $d_r = 1$ μm and $f = 0.15$ with interface debonding, using both our punched zone model and the conventional model, where interface failure is included but the punched zone is not. It can be observed that debonding commences whether or not the punched zone is accounted for in the model. However, the maximum effective plastic strains are located just outside the punched zone/matrix boundary for the model with a punched zone, while they are located just outside the particle–matrix interface for the model without a punched zone. With the punched zone, more debonding takes place along the interface and so more of the load is carried by the punched zone. Therefore, the peak effective plastic strain is formed just outside the punched zone/matrix boundary, where there is a strength discontinuity. Thus, in the presence of a punched zone, the failure initiates by the interface debonding (similar to its conventional counterpart), but then it may continue either by progressive debonding or developing localization or void growth in the matrix.

Fig. 10 is a consolidated plot of all of the strength results that include interface debonding. This figure shows the normalized stress (the composite flow stress

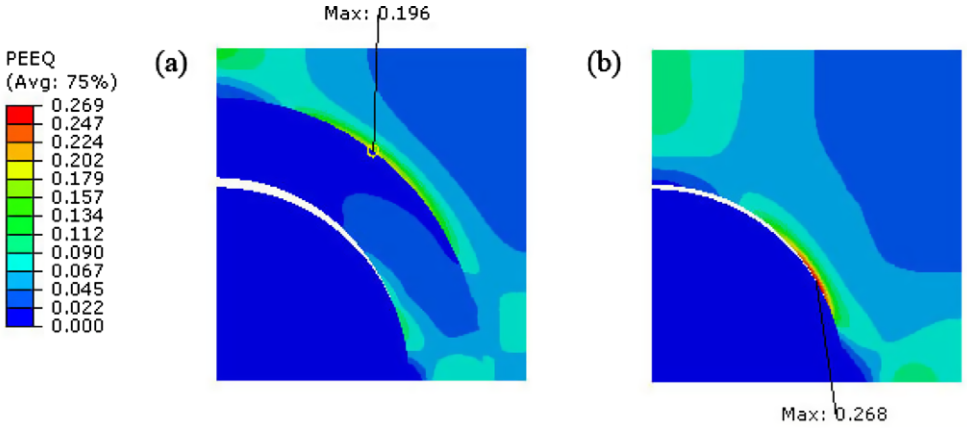

Fig. 9. Equivalent plastic strain contours for a damaging composite containing small 1 μm particles (a) with the punched zone and (b) without the punched zone. The volume fraction is 15% in each case. Note the very different locations of the region of maximum equivalent plastic strain (which likely has implications for matrix failure processes).

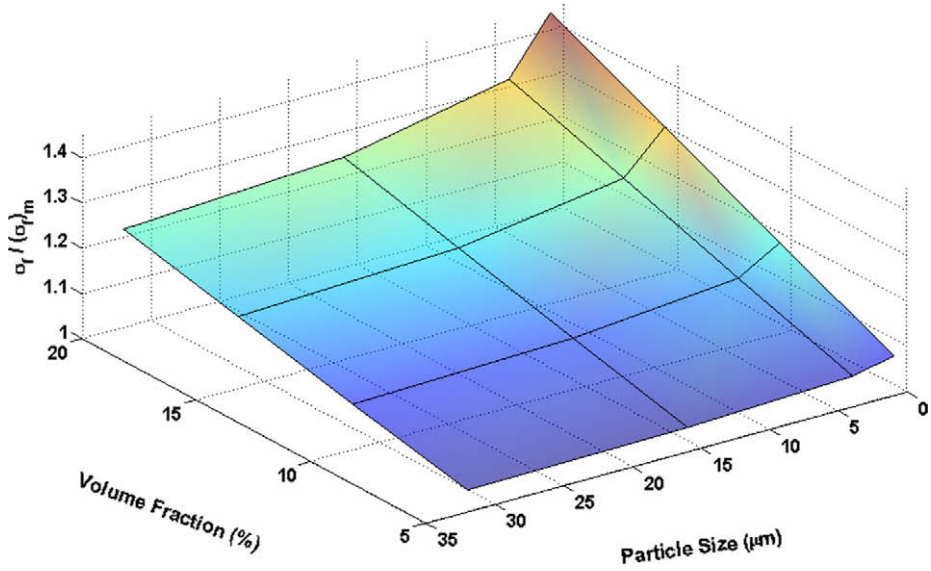

Fig. 10. Normalized composite strength (composite flow stress divided by matrix flow stress at 0.01 strain) as a function of reinforcement volume fraction and particle size in the presence of damage due to interface debonding. The effective strengthening is smaller than in the non-damaging case.

divided by the matrix flow stress at a strain of 0.01) as a function of particle size and volume fraction. Higher stresses for smaller particle sizes and larger volume fractions are still clearly observed, as in the case without debonding (Fig. 6), but the influence of the smaller particles is less dramatic because of damage occurring along the interface. Therefore, the size-dependent strengthening is smaller than that in Fig. 6 (which did not allow for debonding).

5. Implications for materials design

The preceding finite-element calculations demonstrate that the incorporation of the punched zone into the unit-cell model results (as is perhaps to be expected) in the observed size-dependent strengthening in particle-reinforced MMCs and has implications for failure mechanisms. We discuss the implications of these results for materials design in this section.

First, it is useful to define the limits of this approach. Our results do not imply that the progressive reduction of reinforcing particle size will always result in improved mechanical properties such as strength. The model is essentially a continuum model, and ignores the existence of such features as dislocation substructures and grain boundaries in real microstructures. Thus, the model will of necessity breakdown when the particle size becomes comparable to the size scales associated with dislocation patterning inside a grain, or when the particle size becomes comparable to the grain boundary spacing. The temptation to use these results to claim that higher strength will be obtained with extremely fine particles must therefore be resisted. As the particle size is decreased, strengthening mechanisms such as Orowan strengthening and precipitate and dispersoid strengthening should be considered, and it is not immediately clear when the transition will occur between such mechanisms and the enhanced continuum approach presented here (this transition will depend on matrix behavior and matrix microstructure).

With this caveat, it is useful to examine some possible trade-offs in microstructural design for such composites. It is apparent that higher composite strength can be obtained using smaller particles, even with relatively small volume fractions of less than 20%, provided the particle–matrix interface is sufficiently strong. Strengthening increments of around 40% should be achievable by using micron-sized ($\sim$2 μm) particles, even at relatively low volume fractions. The fact that this is not observed very often in the experimental materials created to date is likely due to the difficulties associated with developing uniform dispersions of such fine particles in a matrix, and suggest the need for increased efforts in processing of such materials (indeed, some of the "trimodal" materials created by Schoenung and coworkers [30] are likely to benefit from this strengthening mechanism).

The trade-off associated with increasing the strength by decreasing the particle size is that the stress on the particles and the interfaces increases substantially, leading to the potential for both interface damage and particle fracture. In the case of particle fracture, Figs. 7 and 8 demonstrate that the stress in the particle increases substantially as a result of the presence of the punched zone as the particle size decreases. Thus, the possibility of particle fracture must also be taken into account as the strength of the composite is increased [10,28,31,32]. Assuming that the matrix remains intact (i.e. no void nucleation and growth), and the matrix–particle interfaces remain perfectly bonded, the punched zone surrounding a particle results in higher principal stress in the particle. Further, for fixed f the maximum principal stress is much higher for a smaller particle (e.g. 2 μm) than for a larger particle (e.g. 16 μm). Thus, the likelihood of particle fracture might still exist even for small particles at these volume fractions [31]. Although the fact that the flaw population depends inversely on the particle size (larger particle, smaller fracture stress) will dominate the probability of particle fracture, our computations suggest that particle fracture is also likely to be mediated by the size-dependent stress on the particles due to the presence of punched zones (smaller particles, larger induced principal tensile stress) combined with the volume fraction effect. These aspects are observed in many experimental investigations (e.g. [33]) and have been addressed in some detail for different matrix–particle combinations, but are complicated by issues such as particle shape, angularity and internal defect distribution due to provenance [34]. If particle fracture is assumed to obey a Weibull distribution (e.g. as shown in Refs. [35–38]), it would be useful to look for optimal values of material design parameters such as particle size and volume fraction.

In the case of interface and matrix failure, the presence of the punched zone has a significant influence on the likely failure mechanism. For example, assuming perfect bonding, the equivalent plastic strain distributions in a composite are shown in Fig. 11 for fixed particle size ($d_r = 1$ μm) but varying volume fraction in (a) $f = 5\%$ and (b) $f = 15\%$, and for fixed volume fraction ($f = 20\%$) and varying particle size in (c) $d_r = 1$ μm and (d) $d_r = 16$ μm. In Fig. 11a and b, the location of the maximum equivalent plastic strain moves from just outside the punched zone/matrix boundary to the interface between the matrix and the particle as f increases, for fixed d_r. Thus, the type of failure may transition from a matrix-type failure (e.g. strong shear localization or void nucleation) to an interface-type failure as f increases (for the small 1 μm particles). On the other hand, Fig. 11c and d show that for $f = 20\%$ the plastic strain concentration is always largest at the particle–matrix interface irrespective of the particle size. For the specific case of high f, these observations indicate that for the range of d_r considered here, the size of a particle does not significantly influence the failure mode, and the failure process may be dominated by interface debonding. However, there is a coupling between the d_r and f in determining which mode is likely to initiate failure

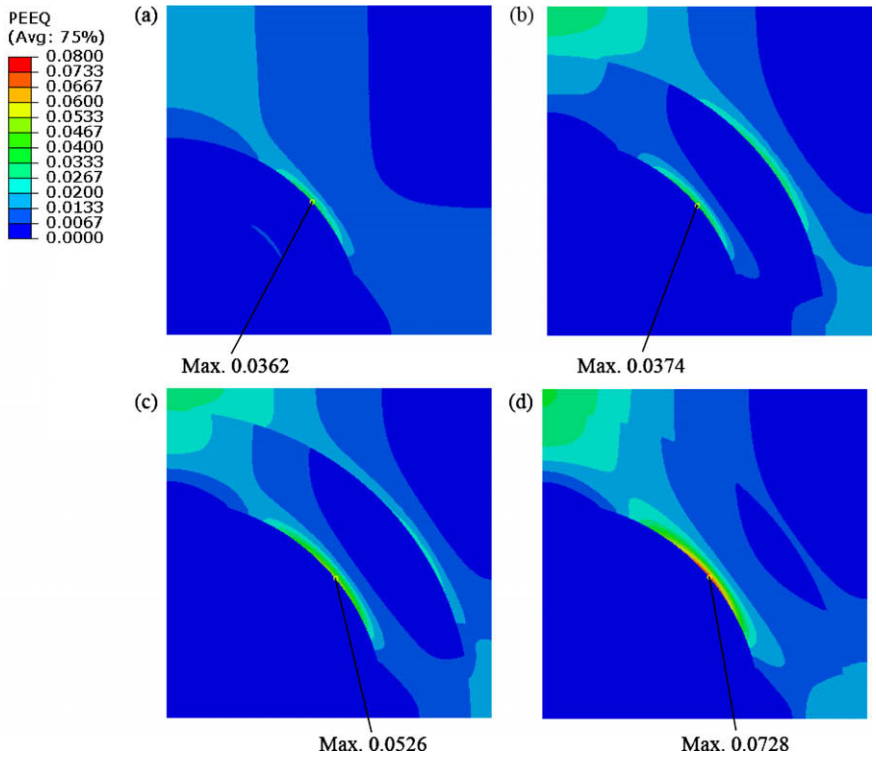

Fig. 11. Effective plastic strain distribution for composites deformed to 0.01 overall strain in tension assuming perfect bonding, for fixed particle diameter ($d_r = 1$ μm) for (a) $f = 5\%$ and (b) $f = 15\%$, and for fixed volume fraction ($f = 20\%$) for (c) $d_r = 1$ μm and (d) $d_r = 16$ μm.

(Fig. 11a and b). Examining Fig. 11a–c, it is apparent that increasing the volume fraction at fixed particle size results in a change in the failure mode. To test this further, we performed a simulation with $d_r = 0.5$ μm and $f = 20\%$ (results not shown here). For this case the plastic strain concentration again occurred at the punched zone–matrix boundary (similar to Fig. 11a). Thus, at fixed volume fraction, as we decrease particle size, a transition occurs from an interface-dominated failure initiation to a matrix-dominated failure initiation. Note that these calculations are for a perfect interface. This suggests that the interfaces tend not to be the first choice of failure for small particle sizes (in the range of 1 μm) and may appear to be stronger simply because there may be alternative mechanisms of damage nucleation due to the particle size effect.

6. Summary

A finite-element-based microstructural modeling technique is presented that incorporates a discrete representation of the punched zones in a matrix with excess dislocation density around reinforcing particles due to CTE mismatch, giving a size-dependent composite strengthening. The elegance of this approach is that it addresses the size-dependent strengthening through appropriate physics while retaining the simplicity of the conventional unit-cell modeling approach, and can be extended to account for different particle shapes. The primary results are the following:

- An equation for the coupling of the size-dependent increase of yield strength of metal matrix composites with the particle volume fraction is presented. Smaller particles lead to greater strengthening, and this size effect is larger for larger volume fractions. At large particle sizes, one recovers the size-insensitive response predicted by conventional plasticity models.
- The stresses inside the reinforcing particles increase as the particle size decreases. This may lead to the potential for particle fracture even for smaller particles, and so using high-quality particles remains important when small particles are used. It may not be sufficient to rely only on the argument that smaller particles are less likely to fracture because of the lower probability of finding flaws.
- The stress in the particles is much higher when the punched zone is accounted for, which means that the strength analysis of the composite may be underestimated if GNDs are not considered.
- When interfacial damage (through debonding) is included in the model, the degree of damage that is induced and the softening that results from damage are found to be dependent on the particle size.
- The analysis indicates that the location of probable failure and the likely failure modes depend on the particle size and the particle volume fraction as well as on the properties of the particle–matrix interface. This suggests some microstructural approaches to controlling the failure mode of MMCs. Our future work will focus on extending this approach to generic particle arrangements and shapes.

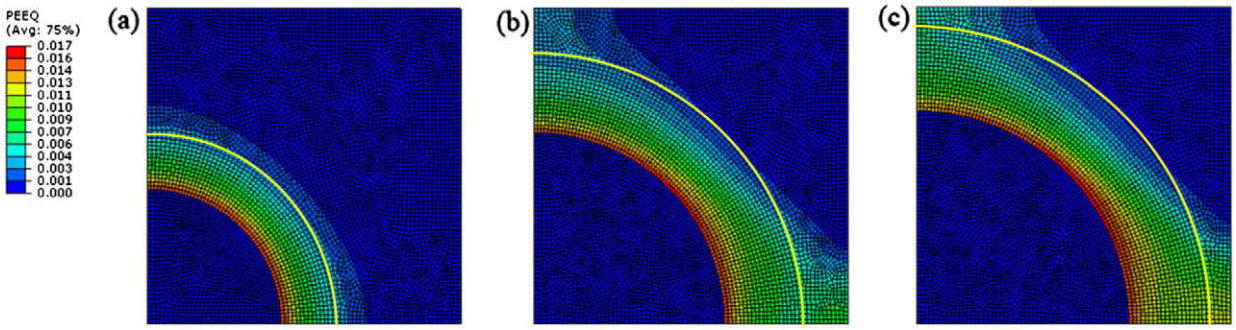

Fig. A1. Finite-element results of effective plastic strain due to thermal mismatch of matrix and particle. The yellow line indicates the analytical plastic zone size according to Shibata et al.'s equations [15]. Temperature decrease is assumed to be 474 K. The unit-cells shown are 16 μm particles with (a) 5%, (b) 15% and (c) 20% volume fractions.

Acknowledgments

S.P.J. acknowledges financial support from NUS through the start-up Grant R-265-000-294-133. This work was performed under the auspices of the Center for Advanced Metallic and Ceramic Systems (CAMCS) at the Johns Hopkins University, supported by the Army Research Laboratory under ARMAC-RTP Cooperative Agreement No.W911NF-06-2-0006. Y.S.S. expresses appreciation to Hannam University for partial support through the 2008 Hannam University Research Fund during his sabbatical at JHU.

Appendix A

A.1. Computational estimate of punched zone size

We develop a continuum numerical prediction of the punched zone size due to thermal mismatch of particles and matrix for comparison with the analytical estimate (Fig. A1). A finite-element calculation was performed of the residual plastic zone around a spherical particle after cooling of the unit-cell from a high temperature (using the same temperature change of 474 K defined earlier). For comparison, ideal plasticity is assumed, as used by Shibata et al. [15]. Traction-free boundary conditions are used on the top and the right-hand side. Fig. A1 shows good agreement between the two approaches, particularly at smaller volume fractions. As the ratio of the punched zone size to the particle size depends only on the material properties and particle volume fraction, this computational corroboration with the analytical punched zone calculation will hold for spherical particles of all the sizes. The finite-element results show that the residual plastic zone may reach the unit-cell boundary for larger volume fractions, and we have used this to define the limits on f for this paper.

The punched zone modeling approach could be made semi-automatic by invoking a User Defined Field (USDFLD) capability in Abaqus [22] that will allow a higher strength to be associated with the punched zone region. While this approach can in principle be extended to more irregular or non-spherical geometries, the calculation of the strengthening contribution will be more involved.

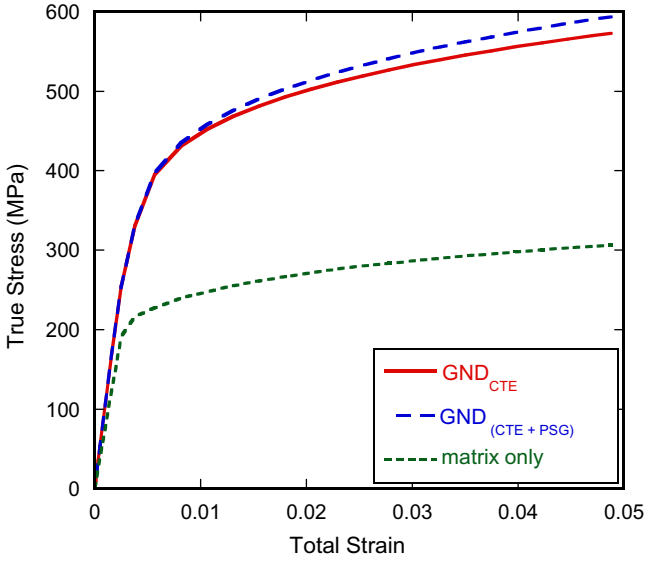

Fig. B1. Influence of the deformation-induced plastic strain gradient on the overall composite response.

Appendix B

B.1. Inclusion of the deformation-induced plastic strain gradient

Following Nan and Clarke [7], the isotropic strengthening ($\Delta\sigma_{psg}$) due to plastic strain gradient is:

$$\Delta\sigma_{psg} = \xi G\left(\frac{f\varepsilon^p b}{d}\right)^{\frac{1}{2}},$$

where $\xi = 0.4$ is a constant, and ε^p is the effective plastic strain. As a first approximation, we superpose this strengthening contribution onto the stress–strain response of the punched zone alone. Fig. B1 shows the true stress–true strain behavior of the 0.5 μm sized composite with

$f = 20\%$ for a perfect interface. The deformation-induced plastic strain gradient does not affect the yield strength of the composite but contributes to the hardening especially at higher strains. For imperfect interfaces this higher hardening may compete with the softening mechanism due to debonding.

References

[1] Arsenault RJ, Shi N. Mater Sci Eng 1986;81:175.
[2] Ling Z, Luo L, Dodd B. J Phys IV: JP 1994:4.
[3] Lloyd DJ. Int Mater Rev 1994;39:1.
[4] Dai LH, Ling Z, Bai YL. Compos Sci Technol 2001;61:1057.
[5] Qu S, Siegmund T, Huang Y, Wu PD, Zhang F, Hwang KC. Compos Sci Technol 2005;65:1244.
[6] Xue Z, Huang Y, Li M. Acta Mater 2002;50:149.
[7] Nan CW, Clarke DR. Acta Mater 1996;44:3801.
[8] Zhang H, Ye J, Joshi SP, Schoenung JM, Chin ESC, Ramesh KT. Scripta Mater 2008;59:1139.
[9] Barlow CY, Hansen N. Acta Metall Mater 1995;43:3633.
[10] Llorca J, Gonzālez C. J Mech Phys Solid 1998;46:1.
[11] Segurado J, Llorca J. Mech Mater 2006;38:873.
[12] Dai LH, Liu LF, Bai YL. Int J Solids Struct 2004;41:5979.
[13] Taggart DG, Bassani JL. Mech Mater 1991;12:63.
[14] Dunand DC, Mortensen A. Acta Metall Mater 1991;39:127.
[15] Shibata S, Taya M, Mori T, Mura T. Acta Metall Mater 1992;40:3141.
[16] Maire E, Lormand G, Gobin PE, Fougeres R. J Phys 1993;3:1849.
[17] Ding K, Weng GJ. J Appl Mech, Trans ASME 1998;65:596.
[18] Zhang WX, Li LX, Wang TJ. Comput Mater Sci 2007;41:145.
[19] Ashby MF. Philos Mag 1970;21:399.
[20] Tanaka K, Narita K, Mori T. Acta Metall 1972;20:297.
[21] Hansen N. Acta Metall 1977;25:863.
[22] Abaqus. Abaqus USER manual. Version 6.8: <www.simulia.com>; 2008.
[23] Bao G, Hutchinson JW, McMeeking RM. Acta Metall Mater 1991;39:1871.
[24] Tvergaard V. Int J Fract 1982:18 237.
[25] McDanels DL. Metall Trans A 1985;16:1105.
[26] Llorca J, Suresh S, Needleman A. Metall Trans A 1992;23:919.
[27] Chawla N, Shen YL. Adv Eng Mater 2001;3:357.
[28] Lloyd DJ. Acta Metall Mater 1991;39:59.
[29] Pandey AB, Majumdar BS, Miracle DB. Metall Mater Trans A: Phys Metall Mater Sci 2000;31:921.
[30] Ye J, Han BQ, Lee Z, Ahn B, Nutt SR, Schoenung JM. Scripta Mater 2005;53:481.
[31] Kouzeli M, Weber L, San Marchi C, Mortensen A. Acta Mater 2001;49:3699.
[32] Mueller R, Rossoll A, Weber L, Bourke MAM, Dunand DC, Mortensen A. Acta Mater 2008;56:4402.
[33] Li Y, Ramesh KT, Chin ESC. Acta Mater 2000;48:1563.
[34] Spowart JE, Miracle DB. Mater Sci Eng A 2003;357:111.
[35] Ayyar A, Crawford GA, Williams JJ, Chawla N. Comput Mater Sci 2008;44:496.
[36] Brechet Y, Embury JD, Tao S, Luo L. Acta Metall Mater 1991;39:1781.
[37] Hauert A, Rossoll A, Mortensen A. J Mech Phys Solids 2009.
[38] Lewis CA, Withers PJ. Acta Metall Mater 1995;43:3685.